Investigation of a scale-up manufacturing approach for nanostructures by using a nanoscale multi-tip diamond tool

Zhen Tong[1,2,4], Xichun Luo[1*], Jining Sun[3], Yingchun Liang[4], Xiangqian Jiang[2]

1 Centre for Precision Manufacturing, Department of Design, Manufacture & Engineering Management, University of Strathclyde, Glasgow G1 1XQ, UK

2 Centre for Precision Technologies, University of Huddersfield, Huddersfield HD1 3DH, UK

3 School of Engineering and Physical Sciences, Heriot-Watt University, Edinburgh EH14 4AS, UK

4 Center for Precision Engineering, Harbin Institute of Technology, Harbin 150001, China

*Email: Xichun.Luo@strath.ac.uk

Abstract

Increasing interest in commercializing functional nanostructured devices heightens the need for cost effective manufacturing approaches for nanostructures. This paper presents an investigation of a scale-up manufacturing approach for nanostructures through diamond turning using a nanoscale multi-tip diamond tool (four tip tool with tip width of 150 nm) fabricated by focused ion beam (FIB). The manufacturing capacity of this new technique is evaluated through a series of cutting trials on copper substrates under different cutting conditions (depth of cut 100–500 nm, spindle speed 12–120 rpm). The machined surface roughness and nanostructure patterns are measured by using a white light interferometer and a scanning electron microscope, respectively. Results show that the form accuracy and integrity of the machined nanostructures were degraded with the increase of the depth of cut and the cutting speed. The burr and the structure damage are two major machining defects. High precision nano-grooves (form error of bottom width < 6.7 %) was achieved when a small depth of cut of 100 nm was used (spindle speed = 12 rpm). Initial tool wear was found at both the clearance cutting edge and the side edges of tool tips after a cutting distance of 2.5 km. Moreover, the nanometric cutting process was emulated by molecular dynamics (MD) simulations. The research findings obtained from MD simulation reveal the underlying mechanism for machining defects and the initialization of tool wear observed in experiments.

(Some figures in this article are in colour only in the electronic version)

Keywords: nanometric cutting; multi-tip tool; nanostructure; molecular dynamics; processing parameters; machining defect.

1. Introduction

Fabrication of periodic micro/nanostructures has drawn great interest in recent years due to their applications in diverse research fields including optics and electronics, solar energy, cell biology, bioengineering and medical science [1-3]. Numerous nanofabrication techniques including optical and electron beam lithography, focused ion beam (FIB) milling, nanoimprinting, femtosecond laser machining have been developed up to date to produce nanostructured devices/materials. However, the extent of these techniques to mass-production of nanostructures in industrial scale for the commercialization of functional nanostructured devices is limited. This is due to the inherent limitations of these techniques, particularly the complex processing step, low processing efficiency or high operational costs.

Diamond turning using multi-tip single crystal diamond tools is a new promising approach to the fabrication of micro/nanostructures by directly replicating micro/nano structures pre-fabricated on the tip of diamond tools onto work substrate surfaces. Periodic micro grooves [4], arrays [5], and diffraction gratings [6] have been successfully obtained by using micro multi-tip tools fabricated by FIB (with tool tip dimensions ranging from 15 μm to 100 μm). Recently, nano-gratings with pitch of 150 nm can be generated by this technique when using nanoscale multi-tip diamond tools [7, 8]. Owing to the unprecedented merits of high throughput, one-step, and highly flexible precision capabilities, diamond turning using nanoscale multi-tip diamond tools has led to the hope for breaking the technical bottleneck for scale-up manufacturing of nanostructures.

Nevertheless, the formation mechanism of nanostructures in using this technique as well as the relationship between the processing parameters and the integrity and accuracy of nanostructures replicated on work substrates remain unclear, which has become a significant barrier to realize the deterministic nanomanufacturing capability. As the tools and the machined structures are in a range of sub-microns or even dozens of nanometres, even tiny (nanometre level) machining defects can degrade the form accuracy of the machined nanostructures. In-depth understanding of the machining process, especially knowing the nanomanufacturing capability under different cutting conditions is of great significance to fully explore the advance of this technique.

On the other hand, molecular dynamics (MD) simulations have been effectively used to address some fundamental issues related to nanometric cutting of copper such as the emulation of the material removal process [9], the cutting heat generated at different cutting speeds [10], the effect of depth of cut [11] and feed rate [9], and the role of friction on tool wear [12, 13]. Recently, the difference of machining nanostructures between using single tip and multi-tip diamond cutting tools has also been reported [14, 15]. In order to bridge the gap between the atomistic and continuum scale, multi-scale modelling method has been developed by hybridizing the FE and MD simulations [16]. These studies have made significant contributions towards the in-depth understanding of the mechanism of nanometric cutting of copper. However, no comprehensive experimental study or theoretical models have been developed, for nanometric cutting, to systematically study the processing technology when using nanoscale multi-tip diamond tools.

This paper therefore reports a series of nanometric cutting trials on copper substrates (under 15 different cutting conditions) using a nanoscale multi-tip diamond tool fabricated by FIB. The focus will be on the influence of operational parameters on the accuracy and the integrity of machined nanostructures as well as the tool wear. Molecular dynamics (MD) simulations were carried out to gain atomistic insight into the work material behaviours during the nanometric cutting process, and to reveal the underlying mechanism for machining defects and the initialization of tool wear observed in experiments.

2. Experimental setup and machining conditions

2.1 Experimental setup

The nanometric face cutting of an oxygen free copper (OFC) wafer (diameter = 50 mm, thickness = 10 mm) were conducted on a diamond turning machine (Precitech Nanoform 250). The procedure of the diamond turning using the nanoscale multi-tip diamond tool and the fabricated samples are illustrated in figure 1.

Three diamond cutting tools were used in the experiment. Before the multi-tip tool cutting, a flat copper substrate surface was prepared by face diamond turning using two normal diamond tools. One conventional roughing tool was used for rough cutting of the copper surface. After the rough cutting, a controlled waviness diamond tool was used to generate the surface with mirror finish. The cutting fluid (CLAIRSOL 330 special kerosine) was applied in these steps.

The nanoscale multi-tip diamond tool (four tips) was then used to generate nano-grooves on the flat copper surface. The multi-tip tool was fabricated on a FIB instrument (FEI Quanta3D FEG) using the divergence compensation method proposed by Sun et al. [7, 17]. The tool had a tip height of 589.8 nm, a tip width of 152.9 nm and a tip base width of 458.5nm with the tip distance being 706 nm (as shown in figure 1 and figure 11 (a)). The geometrical features of the cutting tools are listed in Table 1.

Table 1: Geometrical features of the cutting tools used in the cutting trials.

	Tool nose radius (mm)	Rake angle (°)	Clearance angle (°)	Cutting edge radius
Roughing tool	0.5 mm	0°	10°	Standard
Controlled waviness tool	0.5 mm	0°	10°	Standard
Nanoscale Multi-tip tool	—	0°	10°	40 nm

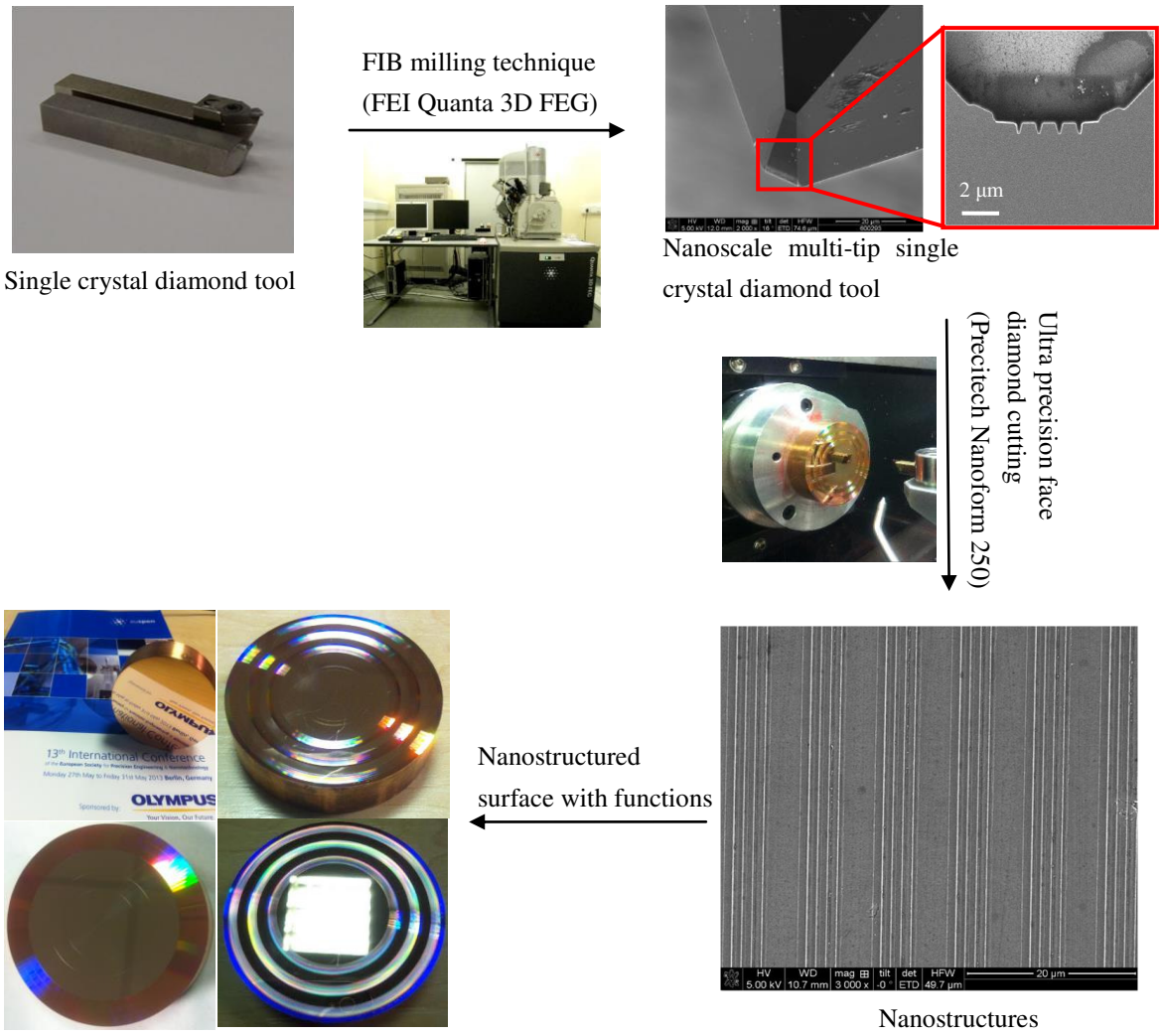

Figure 1: Procedure of diamond turning using nanoscale multi-tip diamond tools.

2.2 Plan for the multi-tip tool cutting

Three spindle speeds tested were 12 rpm (low), 60 rpm (medium), and 120 rpm (high). For each spindle speed, the value of depth of cut was set at five different levels, from 100 nm to 500 nm with an increment of 100 nm. The parameters are listed in Table 2.

The machined surface roughness and the nanostructure pattern were measured by using a white light interferometer (Form TalySurf CCI 3000) and a scanning electron microscope integrated in the FIB system respectively.

Table 2: Operational variables and their levels in face diamond turning trials.

Face cutting	No. of cut	Depth of cut (nm)	Spindle speed (rpm)	Radius of start point (mm)	Cutting speed (m/s)	Feed rate (μm/re)
Group A	1st	100	12	23.0	0.02890	9
	2nd	200	12	22.5	0.02827	9
	3rd	300	12	22.0	0.02765	9
	4th	400	12	21.5	0.02702	9
	5th	500	12	21.0	0.02639	9
Group B	6th	100	60	19.0	0.11938	9
	7th	200	60	18.5	0.11624	9
	8th	300	60	18.0	0.11310	9
	9th	400	60	17.5	0.10996	9
	10th	500	60	17.0	0.10681	9
Group C	11th	100	120	15.0	0.18850	9
	12th	200	120	14.5	0.18221	9
	13th	300	120	14.0	0.17593	9
	14th	400	120	13.5	0.16965	9
	15th	500	120	13.0	0.16336	9

3. MD simulation

3.1 Geometric model for MD simulation

The MD simulation model developed for the study of nanometric cutting using a nanoscale multi-tip diamond tool was shown in figure 2. The geometry of the tool tips was built according to the shape of the multi-tip tool tips fabricated by FIB. The tool had a tip width W_a of $3a_1$ (a_1 = 3.567 Å), a tip base width W_f of $9a_1$, a tool rake angle α of 0º, a tool clearance angle β of 10º, a tip angle θ of 14º, and a cutting edge radius r of $5a_1$. To save the computational time, a double-tip nanoscale diamond tool with the tool tip

distance L of $14a_1$ was employed in present work to represent the nanoscale multi-tip diamond tool (as shown in figure 2(a)). All the tool tips have round cutting edges (a radius r of $5a_1$) as shown in figure 2 (b). The workpiece has a dimension of $50a_2 \times 80a_2 \times 40a_2$ (a_2 = 3.615 Å) and consists of boundary layer and thermostat layer with thicknesses of $2a_2$ and $3a_2$, respectively. Both the nanocrystalline workpiece and the diamond cutting tool were modelled as deformable bodies. The three orientations of the workpiece are [1 0 0], [0 1 0] and [0 0 1] in the X, Y and Z directions (as shown in figure 2 (c)). Free boundary conditions are applied in all directions. The cutting tools are applied along the [-1 0 0] direction on the (0 0 1) surface of the copper. The other computational parameters used in the MD simulations are summarized in Table 3.

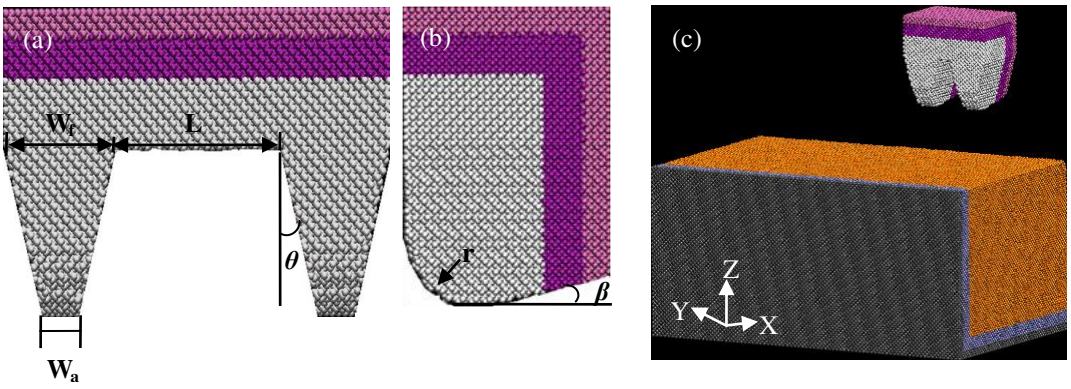

Figure 2: Molecular dynamics simulation model. (a) Front view of the multi-tip tool model; (b) right hand end elevation of the multi-tip tool model; and (c) nanometric cutting model.

Table 3: Simulation parameters of MD nanometric cutting model.

Workpiece materials	Copper
Workpiece dimensions	$50a_2 \times 80a_2 \times 40a_2$ (a_2 = 3.615 Å)
number of atoms	714,707
Time step	1 fs
Initial temperature	293 K
Depth of cut (cutting speed = 200 m/s)	2.0 nm, 2.5 nm, 3.0 nm, 3.5 nm, 4.0 nm
Cutting speed (depth of cut = 2.0 nm)	10 m/s, 50 m/s, 100 m/s, 160 m/s, 200 m/s, 250 m/s

3.2 Potential functions for MD Simulation

In nanometric cutting, hybrid potential functions can be used to describe the interactions between the tool and the workpiece and represent the physical properties of each atoms type being simulated, such as its elastic constants and lattice parameters. For the Cu–Cu interaction the embedded atom method

(EAM) potential proposed by Foiles et al. [18] was used since it has been successfully used in description of metal materials [10] as shown in the following equation:

$$E_{eam} = \sum_{i} F^{i}\left(\sum_{j \neq i}^{n} \rho^{i}(r^{ij})\right) + \frac{1}{2} \sum_{ij, i \neq j} \phi_{ij}(r^{ij}) \quad (1)$$

where the E_{eam} is the total energy of the atomistic system which comprises summation over the atomistic aggregate of the individual embedding energy F^i of atom i and the pair potential ϕ_{ij} between atom i and its neighboring atom j. The lower case superscripts i and j refer to different atoms, r^{ij} is the distance between the atoms i and j, and $\rho^i(r^{ij})$ is the electron density of the atom i contributed by atom j.

For C-C atoms, we adopted Tersoff potential [19, 20] and computed as follows:

$$E_{tersoff} = \frac{1}{2} \sum_{i \neq j} f_C(r_{ij})[\, f_R(r_{ij}) + b_{ij}\, f_A(r_{ij})] \quad (2)$$

where $E_{tersoff}$ is the bond energy of all the atomic bonds, i, j label the atoms of the system, r_{ij} is the length of the ij bond, b_{ij} is the bond order term, f_R is a two-body term and f_A includes the three-body interactions. f_C merely represents a smooth cutoff function to limit the range of the potential.

The Morse potential function [21] was used to describe the interaction between Cu-C and the total energy E_{morse} is expressed as:

$$E_{morse} = \sum_{ij} D_0 \left[e^{-2\alpha(r - r_p)} - 2e^{-\alpha(r - r_p)} \right] \quad (3)$$

where r is the instantaneous distance between atoms i and j. The cohesion energy D_0, the elastic modulus α, and the equilibrium bond distance r_p are 0.087eV, 5.14 $Å^{-1}$, and 2.05 Å respectively.

3.3 MD simulation setup

MD simulations were implemented by using an open source code—LAMMPS [22] compiled on a high performance computing (HPC) workstation using 32 cores. The systems were controlled by NVE ensemble. Before cutting, 85,000 computing time steps were carried out to freely relax the system to 293 K. During cutting, the thermostat atoms were kept at a constant temperature of 293 K using the velocity scaling method to perform the heat dissipation [9]. The cutting speed is applied on the boundary atoms of the cutting tool. The visualization of atomistic configurations was realized by VMD (Visual Molecular

Dynamics) software. The colour scheme of centro-symmetry parameter (CSP) value [14, 23] is indicated in Table 4. The atomistic equivalent temperature [15] was employed to analysis the cutting temperature distributions under different cutting conditions.

Table 4. The default value of atomic defects structure in CSP [14].

CSP value (P)	Lattice Structure	Represent Atoms Colour
3 < P < 5	Partial dislocation	Cyan
5 < P < 8	Stacking fault	Blue
8< P <21.5	Surface atoms	Orange
P> 21.5	Surface edge atoms	Grey

4. Results and discussions

4.1 Nanostructures formed under different cutting conditions

As shown in figure 3 (a), the surface roughness S_a of the copper substrate was 1.85 nm prepared by the face diamond turning. The surface was then machined by the nanoscale multi-tip tool. The SEM images of machined nano-grooves under different depths of cut are shown in figure 4. In general, the periodic nanostructures pre-fabricated on the diamond tool tip were successfully replicated on the copper surface when the depths of cut of 100 nm and 200 nm were used. As shown in figure 4 (a), the measured bottom widths of the nano-grooves generated under the depth of cut 100 nm are ranged from 142.3 nm to 150.2 nm, which are slightly less than the tool tip width of 152.9 nm. The deviation is mainly due to the elastic recovery of the work material after the tool tip released from the surface [7, 14]. Moreover, the surface roughness S_a of the region between each cutting pass was found to be slightly increased to 2.50 nm (as shown in figure 3 (b)), which is mainly caused by the material squeezed from the adjacent cutting passes.

The form accuracy and integrity of the machined nano-grooves were found to be degraded with the increase of depth of cut. Visiable side burrs were observed when the depth of cut was equal or larger than 300 nm (figure 4 (c)). Structure damage was found when a depth of cut of 400 nm was used (figure 4 (d)). The results indicate that there exists an upper limit of depth of cut when machining nano-grooves using nanoscale multi-tip diamond tools.

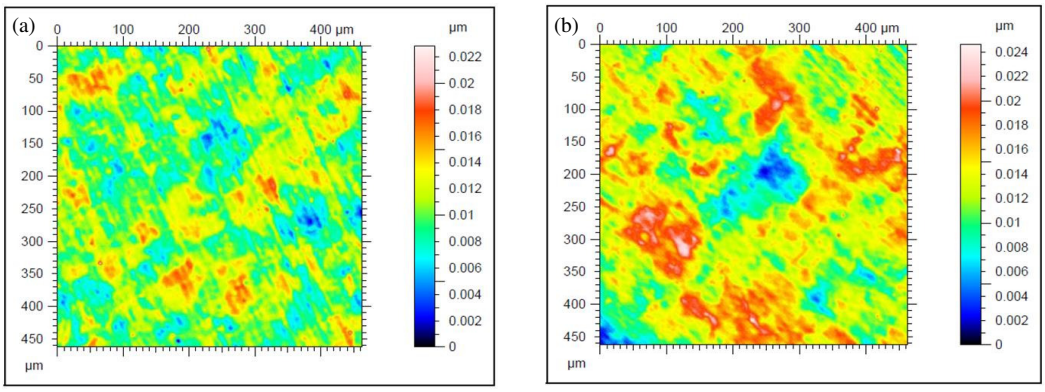

Parameters calculated on the surface before cutting (form removed, polynomial of order 2)

Amplitude Parameters:
S_a = 0.0018541 µm
S_q = 0.0023312 µm
S_z = 0.019278 µm

Parameters calculated on the surface after cutting (form removed, polynomial of order 2)

Amplitude Parameters:
S_a = 0.0025008 µm
S_q = 0.0031812 µm
S_z = 0.019631 µm

Figure 3: The surface roughness of workpiece (a) before nanoscale multi-tip tool cutting, and (b) after nanoscale multi-tip tool cutting (the lens was focused on the surface region between each cutting pass).

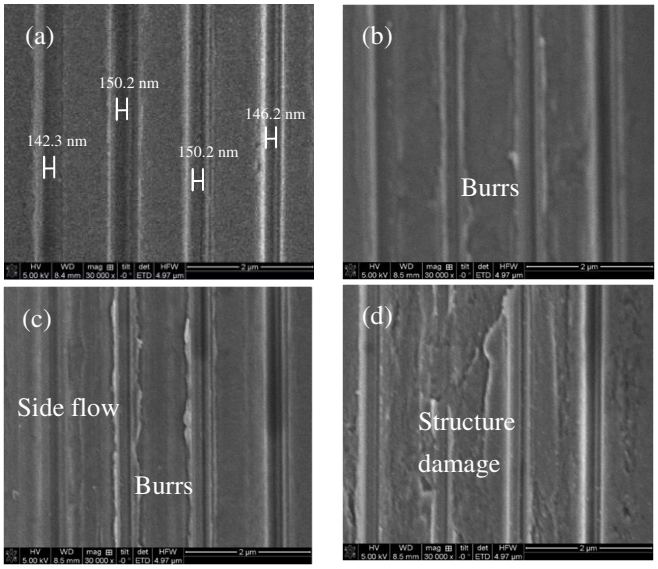

Figure 4: SEM images of nano-grooves machined using different depth of cut. (a) 100 nm; (b) 200 nm; (c) 300 nm; (d) 400 nm. (Spindle speed = 12 rpm, feed rate = 9 µm/re).

The SEM images of nanostructures machined at different spindle speeds are shown in figure 5 (depth of cut = 100 nm). The results show that the form accuracy of the machined nano-grooves degrades with the increase of the cutting speed. No visible defect was found in the case of spindle speed being 12 rpm and 60 rpm. However, side burrs were observed when the spindle speed increased to 120 rpm. A similar cutting speed effect was observed when a depth of cut of 200 nm was used (figure 6). Under a large depth

of cut of 300 nm (figure 7), the increase of cutting speed finally resulted in a seriously structure damage. Therefore, it can be concluded that the burr and the structure damage are the two major types of machining defects when improper processing parameters are used in nanoscale multi-tip tool cutting. The atomistic insight into the work material behaviour responsible for the formation of the machining defects will be discussed in the next section.

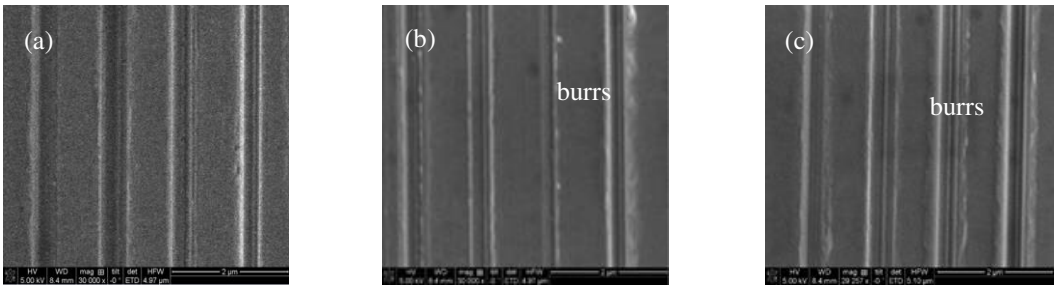

Figure 5: SEM images of nano-grooves machined under different spindle speeds. (a) 12 rpm; (b) 60 rpm; (c) 120 rpm. (Depth of cut = 100 nm, feed rate = 9 μm/re).

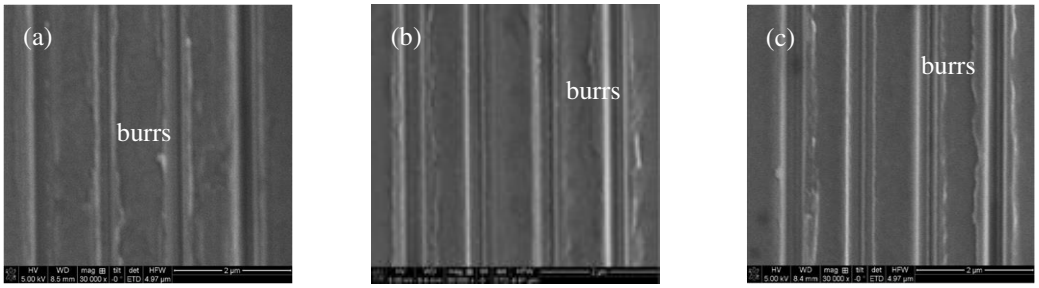

Figure 6: SEM images of nano-grooves machined under different spindle speeds. (a) 12 rpm; (b) 60 rpm; (c) 120 rpm. (Depth of cut = 200 nm, feed rate = 9 μm/re).

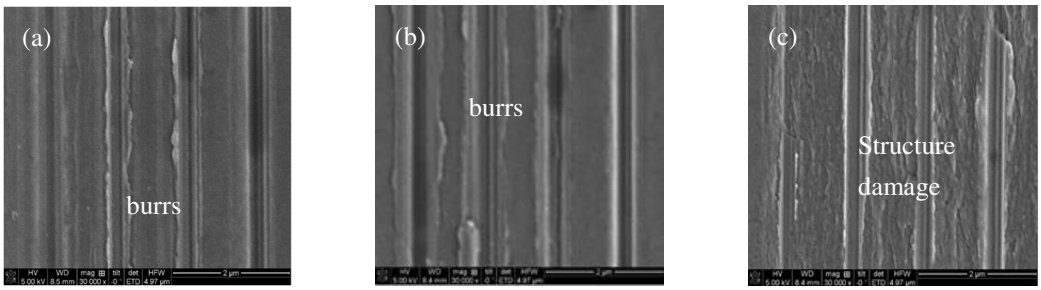

Figure 7: SEM images of nano-grooves machined under different spindle speeds. (a) 12 rpm; (b) 60 rpm; (c) 120 rpm. (Depth of cut = 300 nm, feed rate = 9 μm/re).

4.2 Atomistic observation of nanostructures formation process

4.2.1. Effect of depth of cut

The MD simulation results of machined nanostructures under different depths of cut (cutting speed = 200 m/s) are shown in figure 8. For better comparison, a ratio of depth of cut to tip height (d/h) was employed when comparing the simulation results with experimental results. The quality of the machined nanostructures was characterized by both the form accuracy of the machined nanostructures in depth direction and the thickness of the deformed layers. The form error was calculated by the deviation of the depth of machined nano-groove to the design dimension. As shown in figure 8 (a), two nano-grooves were successfully generated when a depth of cut of 2.0 nm (d/h = 0.46) was applied. However, as evident from figures 8 (b)-(e), the form accuracy is degraded with the further increase of the depth of cut. Apparent side burrs were observed on both edges of the machined nano-grooves. The form divergence of nano-grooves in the depth direction is 4.0% when a depth of cut of 2.5 nm was used. It increased to 8.6% when cutting under a depth of cut of 3.5 nm.

Moreover, the wedge of the cutting tool resulted in material pile-ups around the tool tips. Visible material bulge between the machined nano-grooves was found when a depth of cut of 2.5 nm was used (figure 8 (b)), which mainly due to the overlap effect of the multi-tip tool cutting [8]. However, with further increase of the depth of cut, the height of bulge reduced and it disappeared when a depth of cut of 3.5 nm (d/h = 0.81) was applied (figure 8 (d)). Apparently structure damage was found when a depth of cut of 4.0 nm (d/h = 0.93) was used (figure 8 (e)).

The thicknesses of the deformed layer when using different depths of cut are shown in the middle column of figure 8. Significant dislocation pile-ups were observed beneath the tool tips. The larger the depth of cut, the larger the range of the deformed layer and the dislocations pile-ups were observed. The dislocation pile-ups would result in local strengthening of the work material in the normal direction. The resistance force makes work materials in front of each tip and between the tips flow up [8, 14]. This trend resulted in the built up volume of each cutting tip to merge into one big chip as shown in figures 8 (c)-(e). Due to the emergence of the chip merging, the volume of chip and the height of the tool-chip separation point significantly increased. When the static friction force between the sides of tool tip and the workpiece is large enough, adhesion slip takes place, and results in burrs and structure damages between the tool tips.

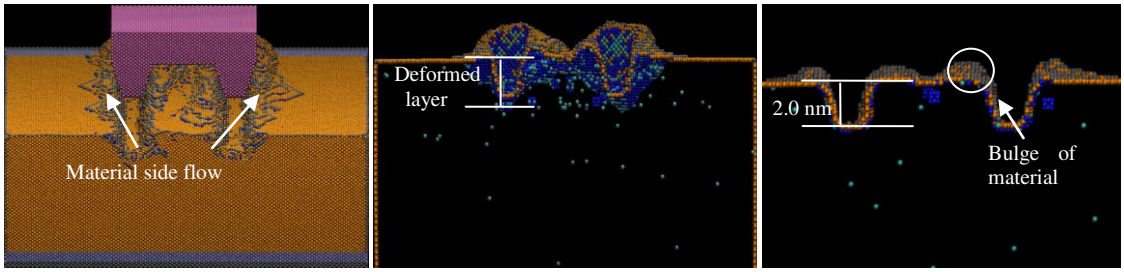

(a) 2.0 nm (d/h = 0.46)

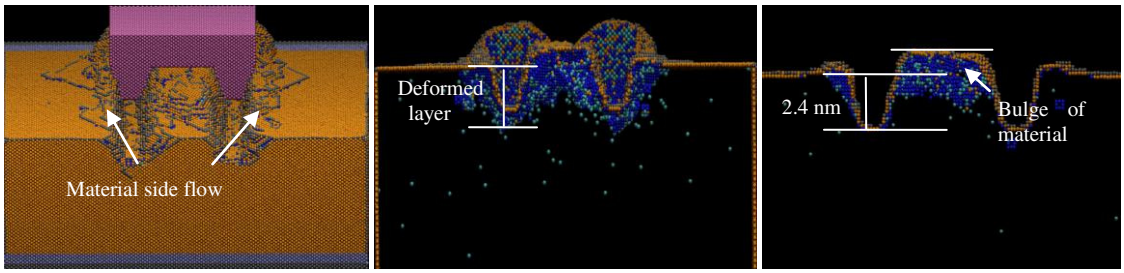

(b) 2.5 nm (d/h = 0.58)

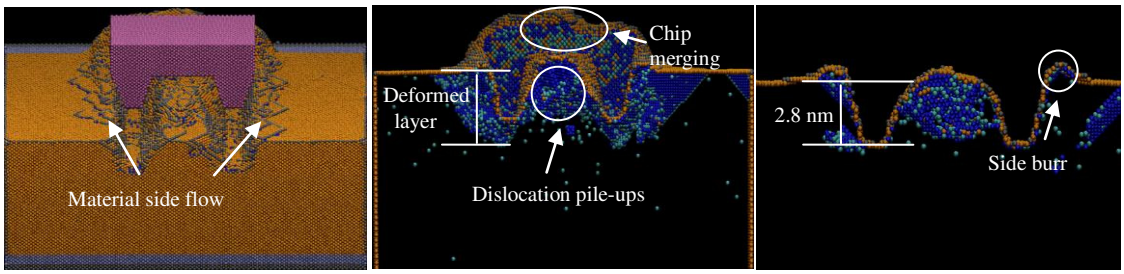

(c) 3.0 nm (d/h = 0.70)

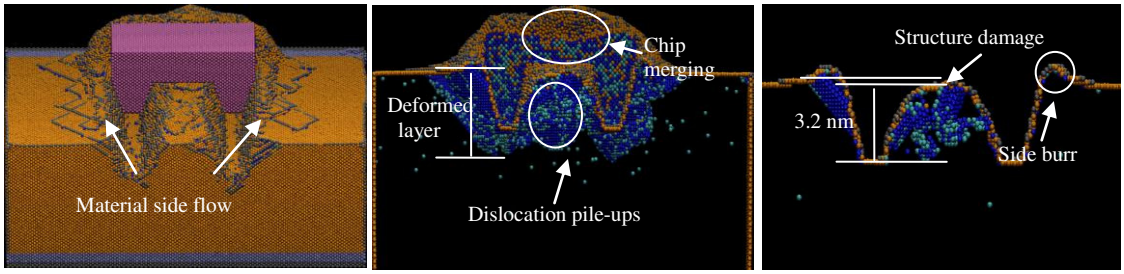

(d) 3.5 nm (d/h = 0.81)

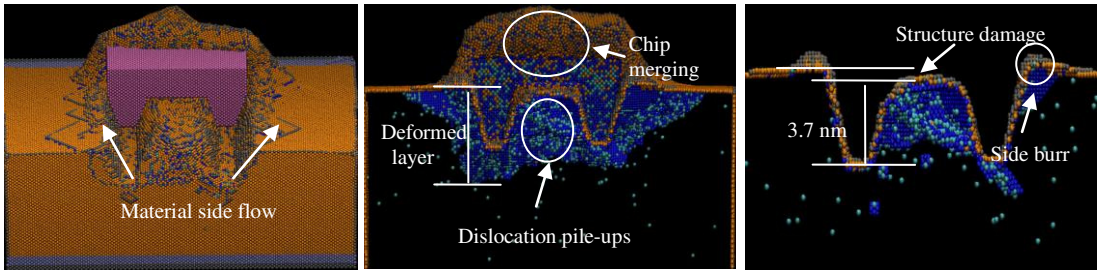

(e) 4.0 nm (d/h = 0.93)

Figure 8: MD simulation results of machined nano-grooves (left), the cross-sectional views of deformed layers (middle), and the cross-sectional views of machined nano-grooves (right) under different depths of cut (cutting speed = 200 m/s): (a) 2.0 nm, (b) 2.5 nm, (c) 3.0 nm, (d) 3.5 nm, (e) 4.0 nm.

In principle, a small depth of cut is a necessary condition of improving the machining precision [24]. The research findings from this work indicate that this rule also applies for the nanoscale multi-tip diamond

tool cutting. In the experimental work (figure 4), the visible structure damage are observed when the depth of cut is equal and larger than 400 nm (d/h = 0.67). In the MD simulation, the critical value of d/h for which the onsets of structure damage is 0.81. It is slightly larger than the experimental result which mainly due to the ideally perfect single crystal structure of copper material and the cutting tool assumed in the MD simulation model.

4.2.2. Effect of cutting speed

In order to obtain in-depth understanding of the effect of cutting speed observed in the experiments, MD simulations of a nanometric cutting process were performed over a wide range of cutting speeds (10–250 m/s) using the same depth of cut of 2.0 nm.

As shown in figure 9, nano-grooves were indicated when the cutting speed was lower than 160 m/s. Although the tiny bulge of materials was observed when the cutting speed increase to 100 m/s, visible side burrs were found when a cutting speed of 250 m/s was applied (figure 9 (e)). Moreover, dislocation pile-ups were found when the cutting speed was equal or higher than 160 m/s (right column of figure 9). This phenomenon indicates that the overlap effect took place when a high cutting speed was used.

Figure 10 summarizes the distributions of local cutting temperatures under different cutting speeds. As expected, the range of the high temperature region (> 450 K) significantly increases with the cutting speed. The high cutting temperature indicated in the high speed cutting softened the work material at the cutting zone and extended the range of material plastic deformation zone, which finally resulted in the overlap effect between the tool tips and the formation of the side burr. Although the cutting speeds used in the MD simulations are still higher than the cutting speeds applied in the experiments, the trend of the cutting speed effect obtained from MD simulations agreed with the experimental results qualitatively. The form accuracy of the machined nano-grooves degraded with the increase of cutting speed.

Nevertheless, it is noted that the cutting speed effect was found to be insignificant when a small depth of cut of 100 nm was used (figure 5). In the MD simulations, the form errors of the machined nanostructures in depth direction are all less than 5% for the cutting speed applied. Visible side burrs were observed only when the dislocation pile-ups took place. Thus it is predicted that, in nanoscale multi-tip tool cutting, there is a critical cutting speed below which the overlap effect can be ignored in machining nanostructures under a certain acceptable accuracy.

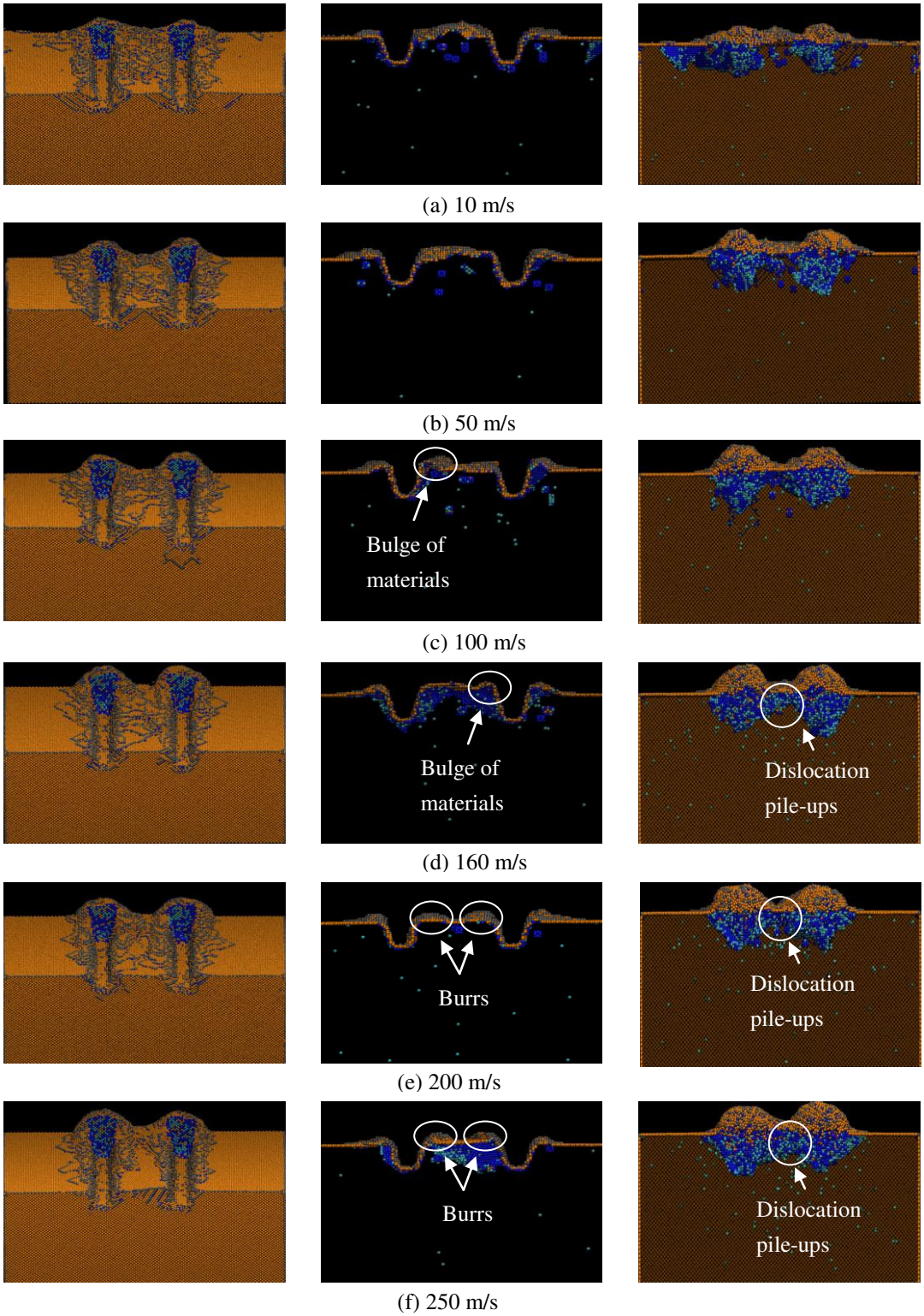

Figure 9: The MD simulation results of nano-grooves formed under the studied cutting speeds. (a) 10 m/s; (b) 50 m/s; (c) 100 m/s; (d) 160 m/s; (e) 200 m/s; (f) 250 m/s. The left column shows the surface of machined nano-grooves; the middle column shows the cross-sectional view of formed nano-grooves; the right column shows the inside view of the dislocation distribution under the cutting tool tips.

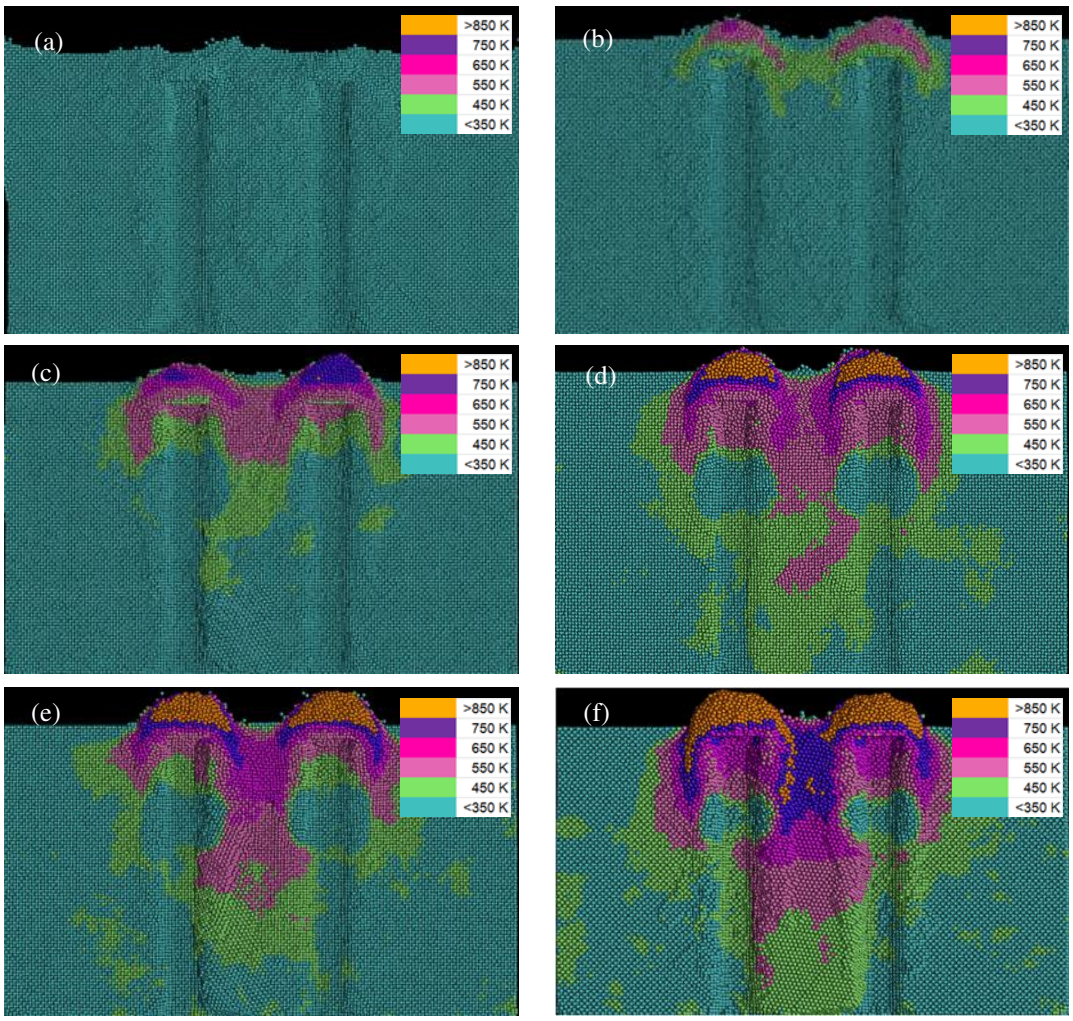

Figure 10: Temperature distribution under different cutting speeds. (a) 10 m/s; (b) 50 m/s; (c) 100 m/s; (d) 160 m/s; (e) 200 m/s; (f) 250 m/s.

4.3 Observation of tool wear

The SEM images of the nanoscale multi-tip tool before and after cutting are shown in figure 11. Unlike the conventional single tip diamond tool cutting where the initial tool wear was mostly found at the clearance face near the tool cutting edges, the tool wear in the multi-tip tool cutting was found on both the clearance face and the sides of the tool tips after a cutting distance of 2.5 km. No visible wear marks were observed at the rake face of the tool tips. The measured tip distance enlarged from 706 nm to 743 nm because of the wear on the sides of the tool tips. The main reason of tool wear is that for multi-tip tool cutting, the nanostructures are formed synchronously within a single cutting pass. The sides of the tool tips are involved in the formation of nanostructures. The compressive stress produced at the sides of the tool tips increases in the friction between the tool tip and workpiece, and thus results in the initiation of

tool wear in this region.

Moreover, the tool wear is closely related to the local cutting temperature [13, 25, 26]. Figures 12 (a)-(c) show the temperature distributions of tool tips under different depths of cut. It is found that the temperature was uniformly distributed at the tool tip when a small depth of cut of 2.0 nm was used. However, a high local temperature (> 620 K) was generated both at the cutting edges and the side edges of the tool tips when cutting under a depth of cut of 3.0 nm. Similar results were observed when the depth of cut increased to 4.0 nm. This high local temperature would soften the C-C bonds strength and accelerate the tool wear process in these regions. In addition, it has been shown in figure 10 that a high cutting speed will apparently increase the cutting temperature at the cutting zone. It is thus anticipated that the tool wear rate will increase with the cutting speed as well.

Theoretically, the tool wear happens in force machining and the wear during the machining of a single part should not exceed the allowable limit [24]. The present study, for the first time, provides the significant information about the initial tool wear of the nanoscale multi-tip diamond tool during the nanometric cutting. More research work are need to be carried out in the future to obtain sufficient data base for building a rigorous tool-life management and predication programme.

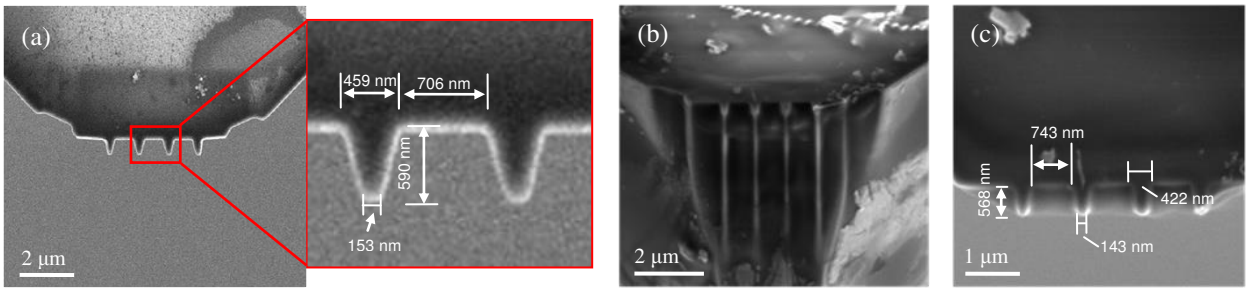

Figure 11: SEM images of the nanoscale multi-tip diamond tool. (a) SEM image of the tool before cutting; (b) SEM image of the tool cutting edges after cutting; and (c) a close up view of the shape of tool tips after cutting.

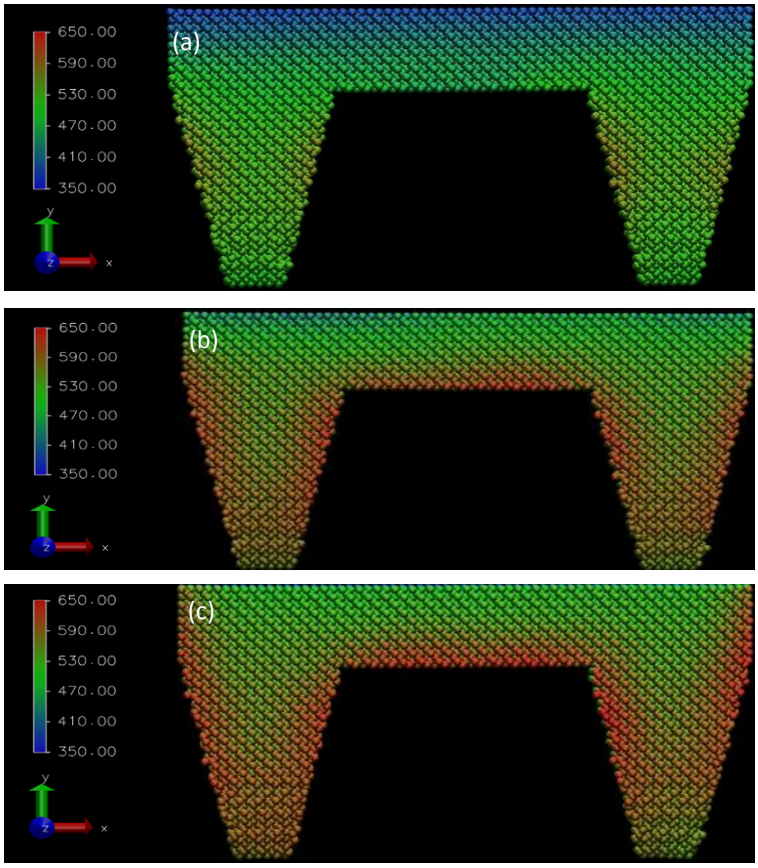

Figure 12: MD simulation results of the temperature distributions on the nanoscale multi-tip diamond tools for different depths of cut. (a) 2 nm; (b) 3.0 nm; and (c) 4.0 nm.

To sum up, due to the limitation of current computational power, performing molecular dynamics (MD) simulation on nanometric cutting with the same physical size and small cutting speed used in experiments remains a big challenge, especially for the large scale MD model built in present work. From experimental side, difficulty has been the limitations of using FIB to fabricate multi-tip diamond tool in several nanometers. It is also lack of detection equipment to capture the transient process of defects formation in nanometric cutting. However, this does not affect our analysis on the general nature of multi-tip tool machining. In this study, the tip geometry of the tool model is a scaled down version of the tool used in experiments. The ratio of depth of cut to tool tip height (d/h) was employed as indicator when comparing the MD simulation results with the experiments. By considering these geometrical details, the simulation results of the formation of machining defects and tool wear were qualitatively compared with the experimental results. The tendency observed from the simulation is in good agreement with the experimental results. The research findings obtained from the MD simulations help interpret the

underlying mechanisms for the machining defects as well as the tool wear during nanometric multi-tip tool cutting process. The present analysis will be valuable to any nanomanufacturing practice where a nanoscale multi-tip diamond tool is used.

5. Conclusions

In this work, experimental studies have been carried out to investigate the nanomanufacturing capacity of using a nanoscale multi-tip diamond tool in conjunction with MD simulations. The conclusions are drawn as follows:

(1) The operational parameters significantly affect the quality of machined nanostructures. High precision nanostructures were successfully produced by face diamond cutting under a depth of cut of 100 nm and a spindle speed of 12 rpm.

(2) Under the studied cutting conditions, the burr and the structure damage are the two major types of the machining defects. The MD simulations indicated that with the increase of the depth of cut and the cutting speed, the increasing overlap effect between tool tips is responsible for the formation of side burrs and structural damages.

(3) The tool wear is initially found at both the clearance cutting edge and the side edges of tool tips after a cutting distance of 2.5 km. The friction produced at the sides of the tool tips and the relatively high local cutting temperature distributed at the tool cutting edges are responsible for the tool wear.

(4) An optimization of the cutting condition, by which the overlap effect can be ignored in the nanostructures generation process, is recommended in the future work to achieve high performance machining of nanostructures when using nanoscale multi-tip diamond tools.

Acknowledgment

The authors gratefully acknowledge the financial support from EPSRC (EP/K018345/1), Sino-UK Higher Education Research Partnership for PhD Studies (CPT508) and the National Funds for Distinguished Young Scholars (No.50925521) of China.

References

[1] S. Holmberg, A. Perebikovsky, L. Kulinsky, and M. Madou, "3-D Micro and Nano Technologies for Improvements in Electrochemical Power Devices," Micromachines, vol. 5, pp. 171-203, 2014.

[2] P. Bartolo, J.-P. Kruth, J. Silva, G. Levy, A. Malshe, K. Rajurkar, et al., "Biomedical production of implants by additive electro-chemical and physical processes," CIRP Annals-Manufacturing Technology, vol. 61, pp. 635-655, 2012.

[3] D. Berman and J. Krim, "Surface science, MEMS and NEMS: Progress and opportunities for surface science research performed on, or by, microdevices," Progress in Surface Science, vol. 88, pp. 171-211, 2013.

[4] Y. N. Picard, D. Adams, M. Vasile, and M. Ritchey, "Focused ion beam-shaped microtools for ultra-precision machining of cylindrical components," Precision Engineering, vol. 27, pp. 59-69, Jan 2003.

[5] X. Ding, G. Lim, C. Cheng, D. L. Butler, K. Shaw, K. Liu, et al., "Fabrication of a micro-size diamond tool using a focused ion beam," Journal of Micromechanics and Microengineering, vol. 18, p. 075017, 2008.

[6] Z. Xu, F. Fang, S. Zhang, X. Zhang, X. Hu, Y. Fu, et al., "Fabrication of micro DOE using micro tools shaped with focused ion beam," Optics express, vol. 18, pp. 8025-8032, 2010.

[7] J. Sun, X. Luo, W. Chang, J. Ritchie, J. Chien, and A. Lee, "Fabrication of periodic nanostructures by single-point diamond turning with focused ion beam built tool tips," Journal of Micromechanics and Microengineering, vol. 22, p. 115014, 2012.

[8] X. Luo, Z. Tong, and Y. Liang, "Investigation of the shape transferability of nanoscale multi-tip diamond tools in the diamond turning of nanostructures," Applied Surface Science, vol. 321, pp. 495-502, 2014.

[9] Y. Yan, T. Sun, S. Dong, and Y. Liang, "Study on effects of the feed on AFM-based nano-scratching process using MD simulation," Computational materials science, vol. 40, pp. 1-5, 2007.

[10] Y. Ye, R. Biswas, J. Morris, A. Bastawros, and A. Chandra, "Molecular dynamics simulation of nanoscale machining of copper," Nanotechnology, vol. 14, p. 390, 2003.

[11] P.-z. Zhu, Y.-z. Hu, T.-b. Ma, and H. Wang, "Study of AFM-based nanometric cutting process using molecular dynamics," Applied Surface Science, vol. 256, pp. 7160-7165, 2010.

[12] Z.-C. Lin and J.-C. Huang, "A study of the estimation method of the cutting force for a conical tool under nanoscale depth of cut by molecular dynamics," Nanotechnology, vol. 19, p. 115701, 2008.

[13] K. Cheng, X. Luo, R. Ward, and R. Holt, "Modeling and simulation of the tool wear in nanometric cutting," Wear, vol. 255, pp. 1427-1432, 2003.

[14] Z. Tong, Y. Liang, X. Jiang, and X. Luo, "An atomistic investigation on the mechanism of machining nanostructures when using single tip and multi-tip diamond tools," Applied Surface Science, vol. 290, pp. 458-465, 2014.

[15] Z. Tong, Y. Liang, X. Yang, and X. Luo, "Investigation on the thermal effects during nanometric cutting process while using nanoscale diamond tools," The International Journal of Advanced Manufacturing Technology, pp. 1-10, 2014.

[16] X. Sun and K. Cheng, "Multi-scale simulation of the nano-metric cutting process," The International Journal of Advanced Manufacturing Technology, vol. 47, pp. 891-901, 2010.

[17] J. Sun and X. Luo, Deterministic Fabrication of Micro-and Nanostructures by Focused Ion Beam: Springer, 2013.

[18] M. S. Daw, S. M. Foiles, and M. I. Baskes, "The embedded-atom method: a review of theory and applications," Materials Science Reports, vol. 9, pp. 251-310, 1993.

[19] J. Tersoff, "New empirical approach for the structure and energy of covalent systems," Physical Review B, vol. 37, p. 6991, 1988.

[20] J. Tersoff, "Modeling solid-state chemistry: Interatomic potentials for multicomponent systems," Physical Review B, vol. 39, p. 5566, 1989.

[21] N. Ikawa, S. Shimada, H. Tanaka, and G. Ohmori, "An atomistic analysis of nanometric chip removal as affected by tool-work interaction in diamond turning," CIRP Annals-Manufacturing Technology, vol. 40, pp. 551-554, 1991.

[22] S. Plimpton, "Fast parallel algorithms for short-range molecular dynamics," Journal of computational physics, vol. 117, pp. 1-19, 1995.

[23] C. L. Kelchner, S. Plimpton, and J. Hamilton, "Dislocation nucleation and defect structure during surface indentation," Physical Review B, vol. 58, p. 11085, 1998.

[24] N. Hiromu, "Principles of precision engineering," Oxford New York Tokyo, Oxford University Press, pp. 191-195, 1994.

[25] N. Kawasegi, T. Niwata, N. Morita, K. Nishimura, and H. Sasaoka, "Improving machining performance of single-crystal diamond tools irradiated by a focused ion beam," Precision Engineering, vol. 38, pp. 174-182, 2014.

[26] N. Ikawa, R. Donaldson, R. Komanduri, W. König, P. McKeown, T. Moriwaki, et al., "Ultraprecision metal cutting—the past, the present and the future," CIRP Annals-Manufacturing Technology, vol. 40, pp. 587-594, 1991.